Stem Cell Reports
Article

OPEN ACCESS

Comparative Quantification of the Surfaceome of Human Multipotent Mesenchymal Progenitor Cells

Rebecca J. Holley,[1] Guangping Tai,[1] Andrew J.K. Williamson,[2] Samuel Taylor,[2] Stuart A. Cain,[1] Stephen M. Richardson,[2] Catherine L.R. Merry,[3] Anthony D. Whetton,[2] Cay M. Kielty,[1,*] and Ann E. Canfield[2,*]

[1]Faculty of Life Sciences
[2]Faculty of Medical and Human Sciences
[3]Faculty of Engineering and Physical Sciences
University of Manchester, Manchester M13 9PT, UK
*Correspondence: cay.kielty@manchester.ac.uk (C.M.K.), ann.canfield@manchester.ac.uk (A.E.C.)
http://dx.doi.org/10.1016/j.stemcr.2015.01.007

SUMMARY

Mesenchymal progenitor cells have great therapeutic potential, yet incomplete characterization of their cell-surface interface limits their clinical exploitation. We have employed subcellular fractionation with quantitative discovery proteomics to define the cell-surface interface proteome of human bone marrow mesenchymal stromal/stem cells (MSCs) and human umbilical cord perivascular cells (HUCPVCs). We compared cell-surface-enriched fractions from MSCs and HUCPVCs (three donors each) with adult mesenchymal fibroblasts using eight-channel isobaric-tagging mass spectrometry, yielding relative quantification on >6,000 proteins with high confidence. This approach identified 186 upregulated mesenchymal progenitor biomarkers. Validation of 10 of these markers, including ROR2, EPHA2, and PLXNA2, confirmed upregulated expression in mesenchymal progenitor populations and distinct roles in progenitor cell proliferation, migration, and differentiation. Our approach has delivered a cell-surface proteome repository that now enables improved selection and characterization of human mesenchymal progenitor populations.

INTRODUCTION

Mesenchymal progenitor cells have major therapeutic potential, exemplified by their beneficial effects in preclinical and phase I/II clinical trials after stroke and myocardial infarction (Honmou et al., 2012; Lee et al., 2009) and in ameliorating immune responses in graft-versus-host disease (Kim et al., 2013). Differentiation of these cells along mesenchymal lineages is a major therapeutic feature (Pittenger et al., 1999). They also secrete a potent mix of soluble factors that can regulate inflammation and stimulate endogenous repair (Prockop, 2013); however, poor definition of their cell-matrix interface limits their clinical value.

In adults, multipotent mesenchymal progenitors reside within perivascular niches, notably bone marrow, adipose tissue, and umbilical cord. Although bone marrow is the most frequent therapeutic source of mesenchymal progenitor cells, isolation is invasive, and cell numbers decline with age. The umbilical cord is an attractive alternative allogeneic source of mesenchymal progenitors, with typically higher progenitor to differentiated cell ratios and increased proliferation rates (Batsali et al., 2013). Bone marrow mesenchymal stromal/stem cells (MSCs) and human umbilical cord perivascular cells (HUCPVCs) display some similar phenotypic and functional characteristics in vitro (Sarugaser et al., 2005), with transcriptome analysis highlighting striking similarities in gene expression (Panepucci et al., 2004). However, cell-type-specific differences are also apparent, making the definition of a progenitor cell challenging. Deciphering their cell-surface proteomes is an essential step in enabling the rigorous selection of progenitor populations and understanding their biology, both essential for controlling cell fate and tissue repair.

Mass spectrometry (MS)-based proteomics is a powerful approach for the comparative analysis of protein expression between cell populations. Global approaches have been used to define the MSC proteome (Delorme et al., 2008; Mareddy et al., 2009; Mindaye et al., 2013a, 2013b) and to track the changes in membrane protein expression upon differentiation (Foster et al., 2005). However, comprehensive identification of specific surface markers has been limited by a lack of enrichment of membrane proteins, insufficient resolution of peptides prior to MS, and inability to compare protein levels between progenitors and differentiated cells.

In this study, we combined enrichment of cell-matrix interface proteins with quantitative MS using eight-plex isobaric tags for relative and absolute quantification (iTRAQ) to compare the proteomes of bone marrow MSCs and HUCPVCs. Our approach identified 186 proteins that were significantly enriched in multiple MSC and HUCPVC cultures compared with differentiated mesenchymal cells (adult human dermal fibroblasts [HDFs]), and 216 proteins that were significantly downregulated. Cell-type-specific protein differences were also quantified. Proteins identified as enriched in bone marrow MSCs and HUCPVCs included

known MSC markers CD106, CD49c, and CD58 and novel markers. Validation of ten markers confirmed their upregulation in MSCs and HUCPVCs, expression in freshly isolated MSCs (bone marrow, adipose, and umbilical cord), and downregulation upon multilineage differentiation. Loss-of-function studies in MSCs demonstrated marker-specific differences in proliferation, migration, and differentiation, indicating that they differentially regulate MSC fate. Thus, we have generated a comprehensive repository of MSC and HUCPVC cell-surface proteins that enables improved cell selection, tracking, and functional analysis.

RESULTS

Characteristics of MSCs, HUCPVCs, and HDFs

First, we compared the expression of known MSC surface markers and multilineage potential of primary bone marrow MSC, HUCPVC, and HDF cultures, each from three donors. MSCs and HUCPVCs expressed the mesenchymal progenitor markers CD73, CD90, and CD166 at similar levels, but not CD14, CD34, or CD45, as expected (Figure 1A). Stro-1 was also expressed weakly by MSCs, yet was absent in HUCPVCs and HDFs (Figure 1A). Under defined culture conditions, MSCs and HUCPVCs differentiated into adipocytes, chondrocytes, and osteocytes (Figure 1B; results using MSCs from a different donor are shown in Figure S1A). HDFs expressed similar levels of CD73, CD90, and CD166 compared with MSCs and HUCPVCs (Figure 1A), but they did not exhibit multipotency (data not shown). Passage 5 MSC or passage 6 HUCPVC cells were used for all experiments, as no difference in marker expression or multipotency was evident compared with early passages (Ball et al., 2012, 2014; Cai et al., 2014).

Enrichment and Validation of the Cell-Matrix Interface

Unbiased hypothesis-generating proteomics is essential for the objective identification of cell-surface markers of mesenchymal progenitor cells. As plasma membrane proteins are at relatively low abundance in whole-cell lysates (Weekes et al., 2010), two approaches were used to increase the likelihood of identifying unique cell-surface markers. First, plasma membranes were enriched using sucrose density ultracentrifugation optimized for cell-surface biomarker studies (Holland et al., 2011) (Figure S1B). The membrane fraction yield was ~0.5%–1% of whole-cell lysate; thus, a large number of starting cells (~5×10^7 cells) was required. Confirmation of plasma membrane enrichment was achieved by blotting for surface markers, including platelet-derived growth factor receptor-β (PDGFRβ), ATPase, and neuropilin-1, with decreased cytoskeletal β-actin observed (Figures 1C and 1D). Other intracellular proteins were unchanged, reduced, or minimally enhanced (Figures S1C and S1D).

Second, proteins present in the cell-matrix interface were enriched by isolating the extracellular matrix (ECM) with associated receptors (Soteriou et al., 2013). The cell layer was removed using ammonium hydroxide (Figures 1E and 1F) and residual matrix solubilized for iTRAQ labeling, with Coomassie blue staining confirming different protein composition compared with whole-cell lysates (Figure 1G). Immunoblotting or immunostaining for ECM proteins fibronectin and fibrillin-1 confirmed their enrichment within matrix fractions (Figures 1F–1H).

Quantitative Proteomic Analysis of the Cell-Matrix Interface

We employed an eight-channel isobaric tagging system with tandem MS to simultaneously compare fractionated proteins from HDFs from two donors (controls) with MSCs and HUCPVCs, each from three donors (Figure 1I). Each individual protein sample was denatured, reduced, alkylated, trypsinized, and labeled with unique isobaric tags (for schematic of iTRAQ method, see Figure S2A). Each set of membrane-enriched or matrix-enriched fractions was combined (i.e., mixing individually iTRAQ-labeled samples together) and separated using reverse-phase high-performance liquid chromatography into 90+ fractions, which were then individually analyzed by MS. This step minimized peptide complexity and increased the likelihood of identifying rare peptides. From membrane-enriched samples, we identified 5,688 proteins (more than peptides/protein and unused score of >1.3), of which 5,489 had quantification (Table S1). From matrix-enriched samples, we identified 1,320 proteins, 1,251 with quantification (Table S2). Distributions of protein ratios for individual MSC donors versus HDFs and for individual HUCPVC donors versus HDFs indicated little variation between donors of the same cell type (Figures 2A, 2B, and S2B–S2D). Some cell-type-specific variations between MSCs and HUCPVCs were, however, apparent (Figures 2C and S2D).

Identification and Validation of Cell-Surface Markers

Using two HDF donors as internal controls enabled the calculation of intra-experiment 95% confidence limits, which allowed us to determine whether a protein was significantly altered in MSCs or HUCPVCs. Practically, this gave values within the membrane-enriched fractions as 1.51 (upregulated proteins) and 0.66 (downregulated proteins) and for matrix-enriched fractions as 1.96 and 0.51, respectively. Comparing MSCs or HUCPVCs against HDF preparations allowed identification of 153 proteins in membrane-enriched and 38 proteins in matrix-enriched fractions that were significantly increased in all MSCs and

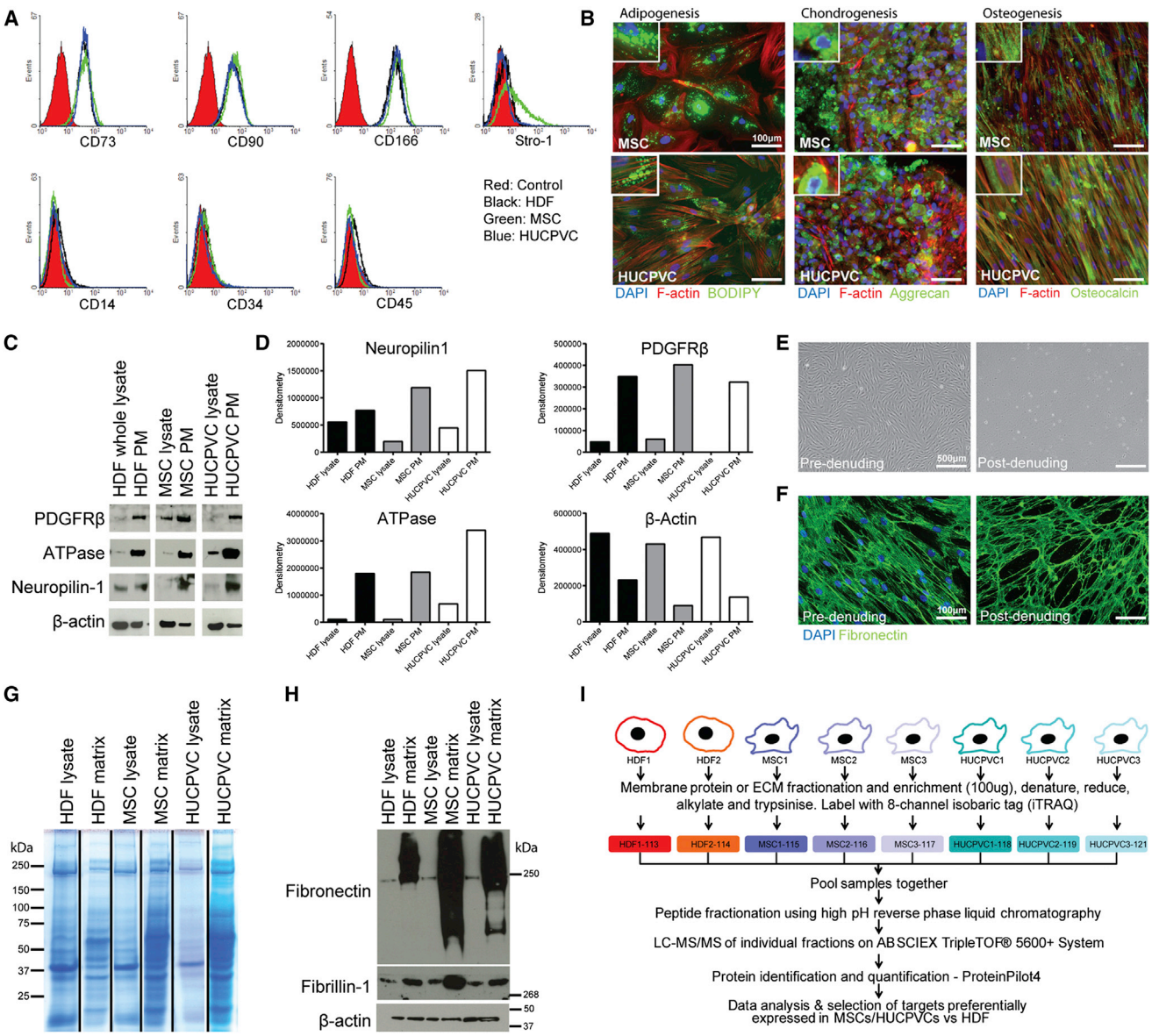

Figure 1. Method to Identify Mesenchymal Progenitor Cell-Specific Markers at the Stem Cell Niche Interface

(A) Flow cytometry for known MSC markers in HDFs (black), MSCs (green), and HUCPVCs (blue). Plots shown are representative of results from three different donor MSC, HUCPVC, and HDF cultures (n = 3). Red filled, isotype control; black line, antibody as indicated.

(B) Immunofluorescence staining for indicated markers (green) after differentiation under adipogenic (16 days), chondrogenic (21 days), and osteogenic (18 days) conditions. DAPI (blue, nuclear); F-actin (red, cytoskeleton). Images are representative of results from three donors (n = 3), with magnified inserts.

(C) Immunoblotting for neuropilin 1, PDGFRβ, ATPase, and β-actin in whole-cell lysate and membrane-enriched (PM) protein samples. Results are representative of three different donor preparations.

(D) Quantification of immunoblot results shown in (C).

(E) Phase images of MSCs pre-denudation and post-denudation.

(F) Fibronectin (green) and DAPI (blue) staining of pre-denuded and post-denuded MSCs.

(G) Coomassie stained gels of whole-cell lysates and matrix-enriched protein samples.

(H) Immunoblotting for fibronectin, fibrillin-1, and β-actin in whole-cell lysates and matrix-enriched protein samples.

(I) Schematic of experimental proteomic workflow. HDF1 and HDF2 represent biological internal replicates with proteins isolated from two donors. Protein samples from three different MSC and HUCPVC donor populations were used.

See also Figure S1.

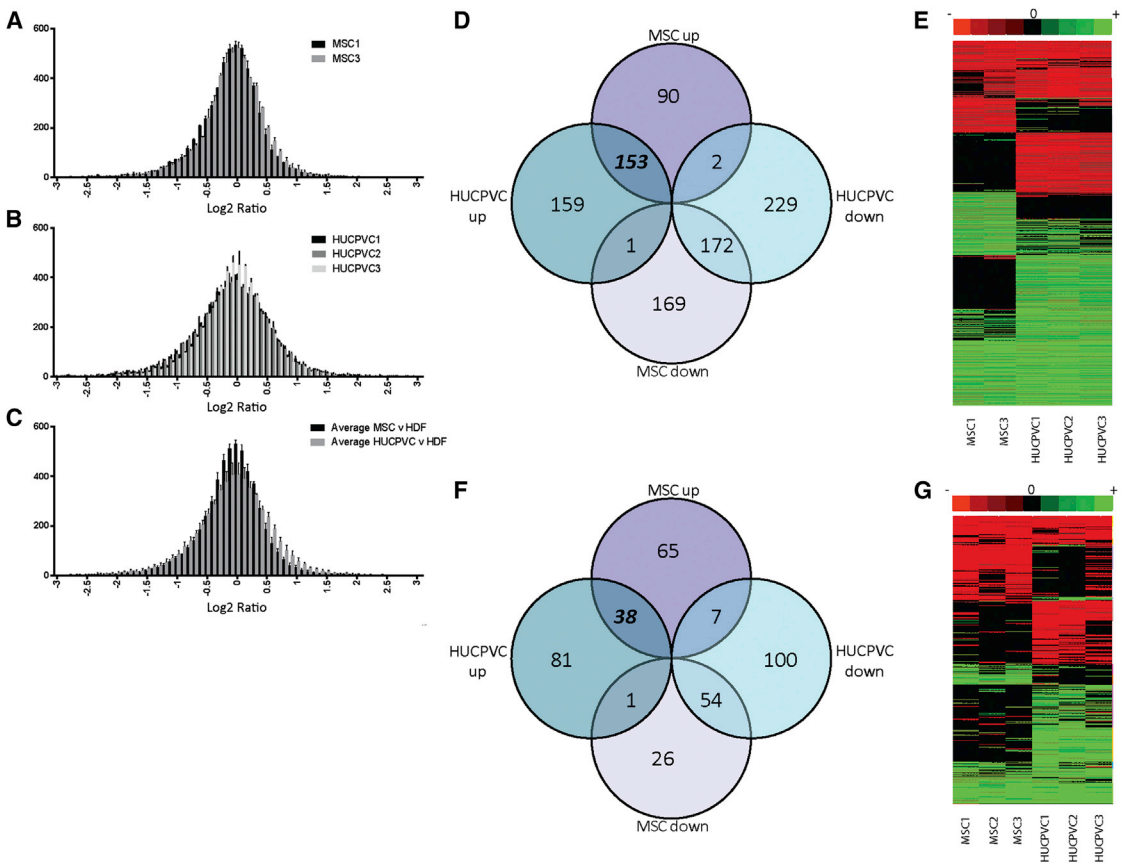

Figure 2. Identification of Mesenchymal Progenitor Cell-Specific Markers Using Eight-Plex Isobaric Tagging and LC-MS/MS

(A and B) Histograms showing the distribution of (log) quantification protein ratios for individual MSC donors versus HDF (A) or HUCPVC donors versus HDF (B) in membrane-enriched fractions. MSC2 was excluded as ITRAQ labeling of this sample was inefficient. Error bars are + SD.

(C) Histogram comparing the distribution (log) of the average protein ratios for MSCs versus HDF and HUCPVCs versus HDF in membrane-enriched fractions. Error bars are + SD.

(D) Venn diagram for membrane-enriched protein fractions illustrating overlapping protein changes seen when comparing all individual MSC cultures versus HDF (MSC up or MSC down) and individual HUCPVC cultures versus HDF (HUCPVC up or HUCPVC down).

(E) Heatmap illustrating clustering of changing genes in membrane-enriched fractions.

(F) Venn diagram for changes seen in matrix-enriched protein fractions.

(G) Heatmap illustrating clustering of changing genes in matrix-enriched fractions.

See also Figure S2.

HUCPVCs versus HDFs (Figure 2D–2E; Tables 1, S3, and S4). Comparing both methods of pre-MS protein enrichment identified that five of these proteins (BGN, SLC3A2, PDLIM5, TINAGL1, and KRT18) were upregulated in both MSCs and HUCPVCs, in both cell fractionation approaches, leading to the combined identification of 186 proteins enriched within progenitor cells.

Our ability to directly compare multiple MSC and HUCPVC samples within the same MS experiment also enabled us to define intra-sample variation between individual cultures. Although numbers of upregulated or downregulated proteins in individual cultures of the same origin versus HDFs varied, a high percentage of proteins were similarly upregulated or downregulated in MSC or HUCPVC cultures (Figures 2E, 2G, and S2E–S2H). For example, comparing each of the three individual HUCPVC cultures in membrane-fractionated samples, >36% of proteins upregulated in one HUCPVC culture were also upregulated in the other two cultures (Figure S2E). Heat maps of significantly altered genes highlight the efficacy of comparing multiple primary cultures (Figures 2E and 2G) to identify global mesenchymal stromal cell markers and eliminate identification of donor-specific proteins.

In the membrane-enriched fractions, 60 of the 153 mesenchymal-specific proteins were identified as plasma membrane proteins (of which 26 had extracellular domains), and 15 were ECM components; the remaining proteins comprised mainly cytoskeletal proteins with membrane connectivity or internal membranous proteins. Gene ontology analysis suggested enrichment of proteins involved in antigen presenting, metabolic and membrane targeting pathways, as well as protein synthesis and degradation (Figure S3). Matrix-enriched fractions provided further information on the composition of the pericellular niche. COL4A1 was enriched in MSC and HUCPVC cultures, and gene ontology suggested alterations in integrins and cytoskeleton composition (Figure S3B).

Our proteomic workflow also identified proteins specifically downregulated within MSC and HUCPVC populations, with 172 proteins identified in membrane-enriched fractions and 54 in matrix-enriched fractions, 10 of which occurred in both analyses (Figures 2D and 2F; Table S5). There was a significant decrease in proteins involved in a multitude of metabolic or transport functions together with niche proteins involved in collagen fibers (e.g., type II collagen α1), microfibrils and elastic fibers (e.g., fibrillin-2, fibulin-2), and basement membranes (e.g., laminin α-4, α-5, β-2).

Several proteins were upregulated in MSCs relative to both HDFs and HUCPVCs (MSC specific) or were identified as HUCPVC specific (Figures 2D and 2F; Tables S6 and S7). These differences likely highlight the different origins of these two mesenchymal stem cell populations. Flow cytometry for membrane proteins BST1 (MSC specific) and CD54 (HUCPVC specific) (Figure 3B) validated these cell-type-specific differences. Notably, only 11 proteins were upregulated in one mesenchymal cell type yet were downregulated in the other.

Identification of Mesenchymal Progenitor Markers

Twenty nine of the 186 proteins specifically enriched within MSCs and HUCPVCs were plasma membrane proteins with extracellular domains (Table 1). Importantly, this group included CD9, ITGA3 (CD49c), CD58, VCAM1 (CD106), MCAM (CD146), and CDH2 (N-cadherin), which are often cited as markers of MSCs. Flow cytometry verified enrichment of these markers in both MSCs and HUCPVCs compared with HDFs (Figure 3A), confirming the efficacy of the relative quantification MS method used. From this dataset, we selected a further ten proteins for validation as progenitor markers: type I transmembrane receptor tyrosine kinase-like orphan receptor 2 ROR2, Eph receptor tyrosine kinase EPHA2, semaphorin co-receptor PLXNA2, atypical member of the cadherin family CDH13 (H-cadherin), transmembrane transporters SLC3A2 and SLC7A5 (heavy and light chains of CD98), endothelial tyrosine kinase TEK (Tie2), disintegrin and metalloproteinase ADAM12, transmembrane transporter SLC39A14, and the proteoglycan biglycan (BGN). Six of these markers, CD98, ROR2, PLXN2, ADAM12, SLC7A2, and CD9, were also identified by Mindaye et al. (2013a, 2013b).

Using flow cytometry and/or immunoblotting, we compared the expression of these proteins in MSCs and HUCPVCs with HDFs, including at least one MSC and HUCPVC donor culture that had not been used in the original MS experiment (Figures 3C and 3D). Smooth muscle cell (SMC) lysates (aortic and coronary) and HUVECs were included in immunoblot analysis to determine whether these markers were also expressed by cells likely to be proximal to the perivascular mesenchymal progenitor cell niche in vivo. This analysis confirmed enrichment for these ten markers within progenitor cell cultures.

To confirm whether the identified protein markers were expressed by tissue mesenchymal progenitor cells, we performed flow cytometry on freshly isolated HUCPVCs (passage 0, released from perivascular regions of the umbilical cord with collagenase; Ennis et al., 2008) or bone marrow MSCs (passage 0 [n = 3 donors], after replating of fractionated mononuclear cells on tissue culture plastic; Strassburg et al., 2010). These cells expressed similar high levels of the markers EPHA2, TEK, CDH13, and CD98 by flow cytometry to the MSCs and HUCPVCs at passages 5 and 6 (compare Figure 3C with Figures 4A, 4B, S4A, and S4B). Flow cytometry for these markers was performed on MSCs derived from subcutaneous fat (adipose tissue-derived MSCs, an alternative MSC source) of matched donors at passage 0 (n = 3 donors; Figures 4C, S4C, and S4D). Analysis confirmed expression of CD9, CD98, ROR2, EPHA2 PLXNA2, and CDH13 alongside known mesenchymal markers, including CD73, CD90, and CD105 in adipose-derived MSCs. We also used flow cytometry to determine the percentage of cells in the mononuclear fraction of freshly isolated bone marrow aspirates, which expressed ROR2, PLXNA2, and CDH13. This analysis revealed restriction of expression of these markers to a small subset of cells (<0.4%), which also expressed the known MSC marker CD105 (Figures S4E–S4I).

To determine whether mRNA expression correlated with protein levels, we used real-time qPCR to compare MSC and HUCPVC mRNA levels with HDFs (Figure 3E). Significant increases in the mRNA levels of *EPHA2*, *SLC3A2*, *SLC7A5*, and *TEK* were shown. However, minimal changes in mRNA levels of *PLXNA2* and *CDH13* were detected, highlighting the need for proteomics alongside mRNA expression.

To determine whether these markers were also downregulated as progenitor cells commit to differentiation,

Table 1. Proteins with Extracellular Domains Identified in Proteomics Screen that Are Significantly Enriched in Mesenchymal Progenitor Cells

Accession Number	Gene Symbol	Name	HDF1 versus HDF2[a]	Average MSC versus HDF[a]	Average HUCPVC versus HDF[a]
ENSP00000264036	MCAM	cell-surface glycoprotein MUC18	1.00	3.21 (0.15)	3.64 (0.64)
ENSP00000294728	VCAM1	vascular cell adhesion protein 1	1.11	3.34 (0.25)	2.08 (0.50)
ENSP00000371958	CD9	CD9 antigen	1.11	3.41 (0.48)	4.4 (0.86)
ENSP00000432773	CD58	CD58 molecule	0.85	1.79 (0.27)	2.15 (0.39)
ENSP00000269141	CDH2	cadherin-2, N-cadherin	0.97	1.9 (0.15)	1.78 (0.28)
ENSP00000439248	ITGA3	integrin, alpha 3 antigen CD49C	0.90	1.68 (0.29)	1.66 (0.17)
ENSP00000428337	TEK	TEK tyrosine kinase, CD202b, Tie2	0.97	1.99 (0.25)	3.13 (0.60)
ENSP00000351209	EPHA2	ephrin type A receptor 2	0.98	2.13 (0.14)	1.95 (0.12)
ENSP00000357668	ADAM12	disintegrin and metalloproteinase domain-containing protein 12	0.99	1.81 (0.31)	2.19 (0.55)
ENSP00000240095	SLC39A14	solute carrier family 39 (zinc transporter), member 14	0.83	2.23 (0.38)	1.97 (0.54)
ENSP00000261622	SLC7A5	solute carrier family 7 (amino acid transporter light chain, L system), member 5; CD98LC	0.84	3.63 (0.37)	4.68 (2.12)
ENSP00000340815	SLC3A2	4F2 cell-surface antigen heavy chain, CD98HC, solute carrier family 3 member 2	0.89	2.55 (0.18)	2.64 (0.69)
ENSP00000387253	SLC20A1	solute carrier family 20 (phosphate transporter), member 1	1.17	1.63 (0.11)	2.64 (0.34)
ENSP00000444408	SLC1A5	solute carrier family 1 (neutral amino acid transporter), member 5	0.80	2.15 (0.31)	1.65 (0.23)
ENSP00000377524	LRFN4	leucine-rich repeat and fibronectin type III domain containing 4	0.79	1.82 (0.27)	3.02 (0.67)
ENSP00000437639	LDLR	low-density lipoprotein receptor	1.15	1.64 (0.28)	2.14 (0.48)
ENSP00000403082	C3orf75	uncharacterized protein	1.15	1.61 (0.39)	2.06 (0.29)
ENSP00000356000	PLXNA2	plexin-A2	1.13	1.83 (0.12)	1.51 (0.34)
ENSP00000445108	GPRC5B	G-protein-coupled receptor, family C, group 5, member B	0.93	1.71 (0.34)	4.62 (0.58)
ENSP00000366157	GPR180	integral membrane protein GPR180	0.99	1.52 (0.11)	2.53 (0.37)
ENSP00000375989	SLC22A3	organic cation transporter 3	0.99	3.22 (0.31)	3.78 (2.81)
ENSP00000364860	ROR2	tyrosine-protein kinase transmembrane receptor ROR2	0.98	1.62 (0.53)	2.58 (0.23)
ENSP00000394557	CDH13	cadherin-13; H-cadherin	0.97	4.6 (0.32)	1.66 (0.33)
ENSP00000438512	THSD1	thrombospondin, type I, domain containing 1	0.95	2.28 (0.71)	1.73 (0.40)
ENSP00000339686	CD82	CD82; uncharacterized protein	0.77	1.56 (0.35)	2.2 (0.81)
ENSP00000280612	SLC7A11	cysteine/glutamate transporter	0.82	1.55 (0.41)	2.12 (0.47)
ENSP00000359223	BGN	biglycan	1.06	2.05 (0.13)	1.62 (0.30)

(*Continued on next page*)

Table 1. *Continued*

Accession Number	Gene Symbol	Name	HDF1 versus HDF2[a]	Average MSC versus HDF[a]	Average HUCPVC versus HDF[a]
ENSP00000327336	BGN	biglycan[b]	1.171	13.17 (7.10)	3.66 (2.23)
ENSP00000386896	ITGA6	integrin alpha-6[b]	0.511	2.74 (1.47)	3.25 (1.26)
ENSP00000319281	BASP1	brain acid soluble protein 1[b]	0.86	2.09 (0.3)	1.76 (0.56)
ENSP00000444236	SLC3A2	4F2 cell-surface antigen heavy chain, CD98HC, solute carrier family 3 member 2[b]	1.271	1.99 (0.44)	2.60 (1.00)

[a]iTRAQ scores >1.51 and >1.96 in membrane-enriched and matrix-enriched fractions, respectively, are significantly upregulated proteins. HDF1 v HDF2 iTRAQ ratios act as an internal control.
[b]Proteins were identified from matrix-enriched fractions; all other proteins were identified from membrane-enriched fractions. See also Tables S1, S2, S3, S4, S5, S6, and S7.

MSCs were differentiated into adipocytes, chondrocytes, or osteoblasts (Figure 1B), and protein levels pre-differentiation and post-differentiation compared by immunoblotting (Figure 3F). For all proteins investigated, expression was markedly reduced after differentiation along all three lineages. These results confirm that these markers reflect the multipotent mesenchymal state and are decreased in expression once cells commit to differentiation.

Investigating Marker Function in MSCs by siRNA

Using an siRNA approach, we investigated how each of the transmembrane molecules ROR2, EPHA2, PLXNA2, CDH13, SLC3A2, and SLC7A5 and the known mesenchymal marker CD9 influence MSC fate. qPCR, immunoblotting, and/or flow cytometry were used to confirm efficient mRNA and protein knockdown (Figures 5A–5G). Changes in MSC morphology were apparent 3 to 5 days after siRNA treatments, with marked alterations clearly visible by day 7 (Figure 5H). The most dramatic shape changes were noted after depletion of CD9 or EPHA2, which resulted in the cells becoming elongated. Cells depleted of ROR2 became large and flattened (Figure 5H). Knockdown of SLC3A2 and SLC7A5 had little effect, with cells remaining spindle shaped.

Proliferation assays demonstrated that cell numbers were significantly reduced after CD9, ROR2, and EPHA2 siRNA treatments, all resulting in a 74%–77% reduction in growth by day 8, compared with cells treated with control siRNA (Figure 5I). Proliferation was less affected after knockdown of PLXNA2, SLC3A2, and SLC7A5 (~50% reduction) or CDH13 (25%).

A therapeutic feature of MSCs is their mobilization to sites of damage, in response to injury, where they participate in repair. We used a wound assay to investigate whether cellular migration was affected after knockdown of these proteins (Figure 5J). A small but statistically significant decrease in migration was detected after PLXNA2 and EPHA2 siRNA treatments. However, CD9 and ROR2 knockdowns caused significant migration defects, with only 62% and 46% wound coverage at 24 hr, respectively, compared with 96% after control siRNA treatment. No effect on cell migration was apparent after CDH13 knockdown (Figure 5J) or with SLC3A2 or SLC7A5 (data not shown). Extensive analysis of cell migration at subconfluence, using live cell imaging to track large numbers of individual cells for 48 hr to 6 days after siRNA knockdown, revealed similar effects (data not shown).

To investigate whether morphological changes after siRNA reflected phenotypic alterations, cells were first immunostained with phalloidin and vinculin to highlight F-actin organization and focal adhesions (Figure 6A). This analysis confirmed gross elongation after CD9 and EPHA2 knockdown, with F-actin staining emphasizing increases in cell length compared with control siRNA-treated cells. There was also a marked decrease in focal adhesion formation in both knockdown cultures. Despite an obvious increase in the area of ROR2 siRNA-treated cells, F-actin and vinculin organization appeared similar to control cells. SLC3A2 and SLC7A5 siRNAs had no apparent effects on these features (data not shown).

Second, we used cell image analysis software (CellProfiler) to quantify size and shape (Figures 6B–6G), after staining of cells with wheat germ agglutinin and F-actin (Figure S5) (Ball et al., 2012). Since cell density can affect cell shape, MSCs were plated at matching densities and allowed to attach for 24 hr prior to analysis. Increased length/width ratios were visible after CD9 and EPHA2 knockdowns (Figure 6D), confirming cell elongation. This linearity was further verified by significant changes in eccentricity (circle = 0, line = 1), extent, and form factor in CD9 and EPHA2 siRNA-treated cells compared with controls (Figure 6E). Area measurements emphasized the greater than 2-fold increase in cytoplasmic area in ROR2 knockdown cells versus controls (Figure 6F), with a 33% decrease in nuclear/cytoplasm ratio (Figure 6G). A 1.8-fold increase in cytoplasmic area was also apparent after PLXNA2 and

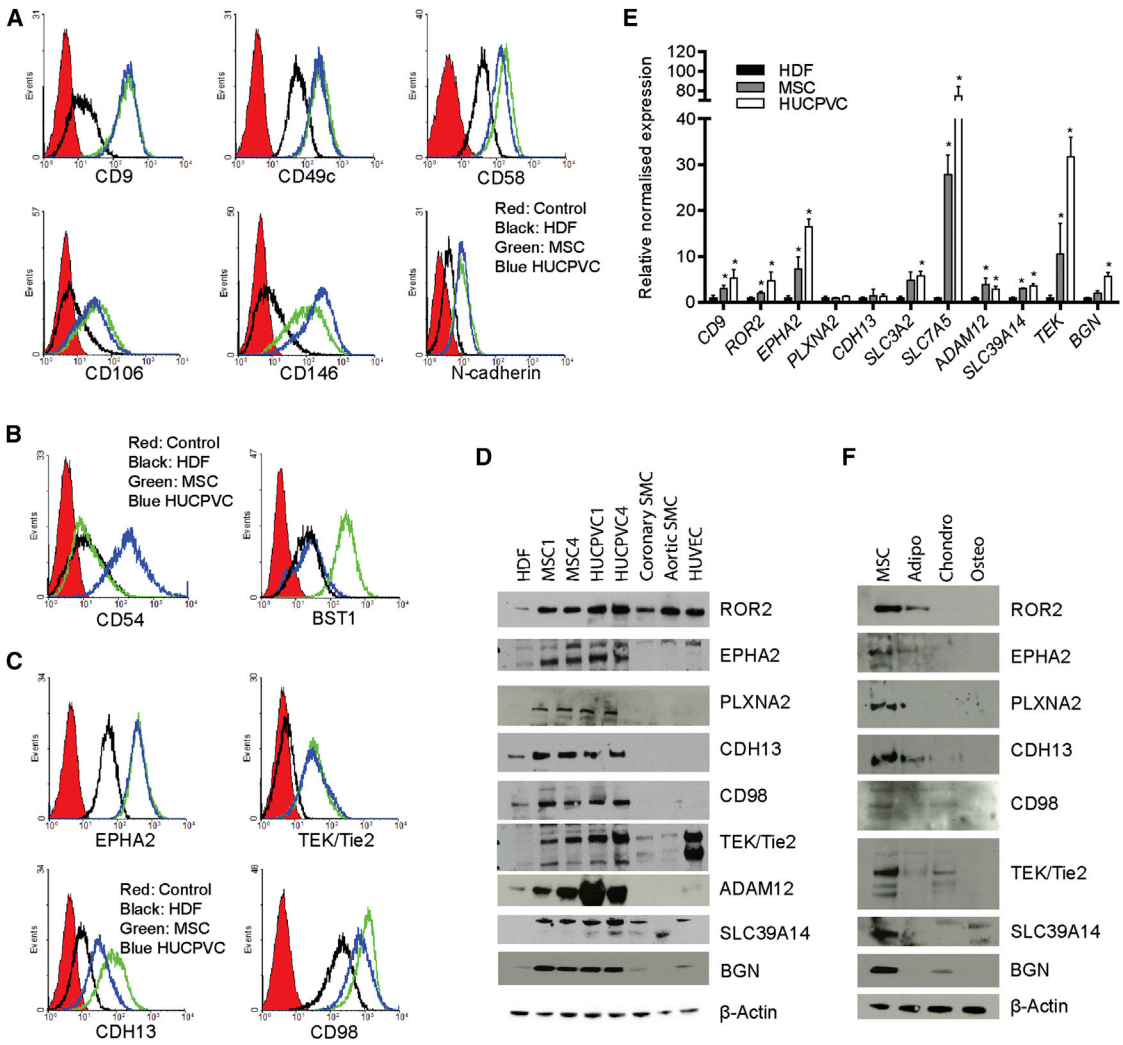

Figure 3. Validation of Mesenchymal Progenitor Cell Targets

(A) Flow cytometry for known mesenchymal progenitor cell markers identified as being enriched within both MSCs and HUCPVCs in the eight-plex iTRAQ LC-MS/MS experiment. Plots are representative profiles from MSC, HUCPVC, and HDF cultures (n = 3–4 donors of each cell type).

(B) Flow cytometry for CD54 and BST1 in MSC, HUCPVC, and HDF cultures. Plots are representative profiles (n = 3–4 donors of each cell type).

(C) Flow cytometry validation of EPHA2, TEK, CDH13, and CD98 identified to be enriched within mesenchymal progenitor populations by MS. Plots are representative profiles (n = 3–4 donors of each cell type).

(D) Immunoblot validation of new markers identified to be enriched within mesenchymal progenitor populations by MS. Blots show protein extracts from HDF, two MSC donors, two HUCPVC donors, human coronary artery, and aortic SMC and HUVEC cultures.

(E) qRT-PCR for markers identified to be enriched within mesenchymal progenitor populations. Results are averages with error bars representing SEM. Expression was normalized relative to housekeeper genes *TBP* and *β2M*, using averages from three individual HDF, four MSC, and four HUCPVC donors.

(F) Immunoblots showing expression of new markers by MSC cultured under normal growth conditions (MSC) or under adipogenic conditions (adipo, 21 days) in pellet chondrogenic conditions (chondro, 24 days) or osteogenic conditions (osteo, 24 days). Blots are representative of results from two donor MSCs.

See also Figure S3.

CD9 knockdown, with smaller (1.3- to 1.4-fold) increases detected as a result of EPHA2 and CDH13 knockdowns (Figure 6F). Thus, whereas all siRNA treatments increased cell size, CD9 and EPHA2 depletion induced significantly elongated phenotypes, and ROR2 depletion resulted in larger, more rounded cells.

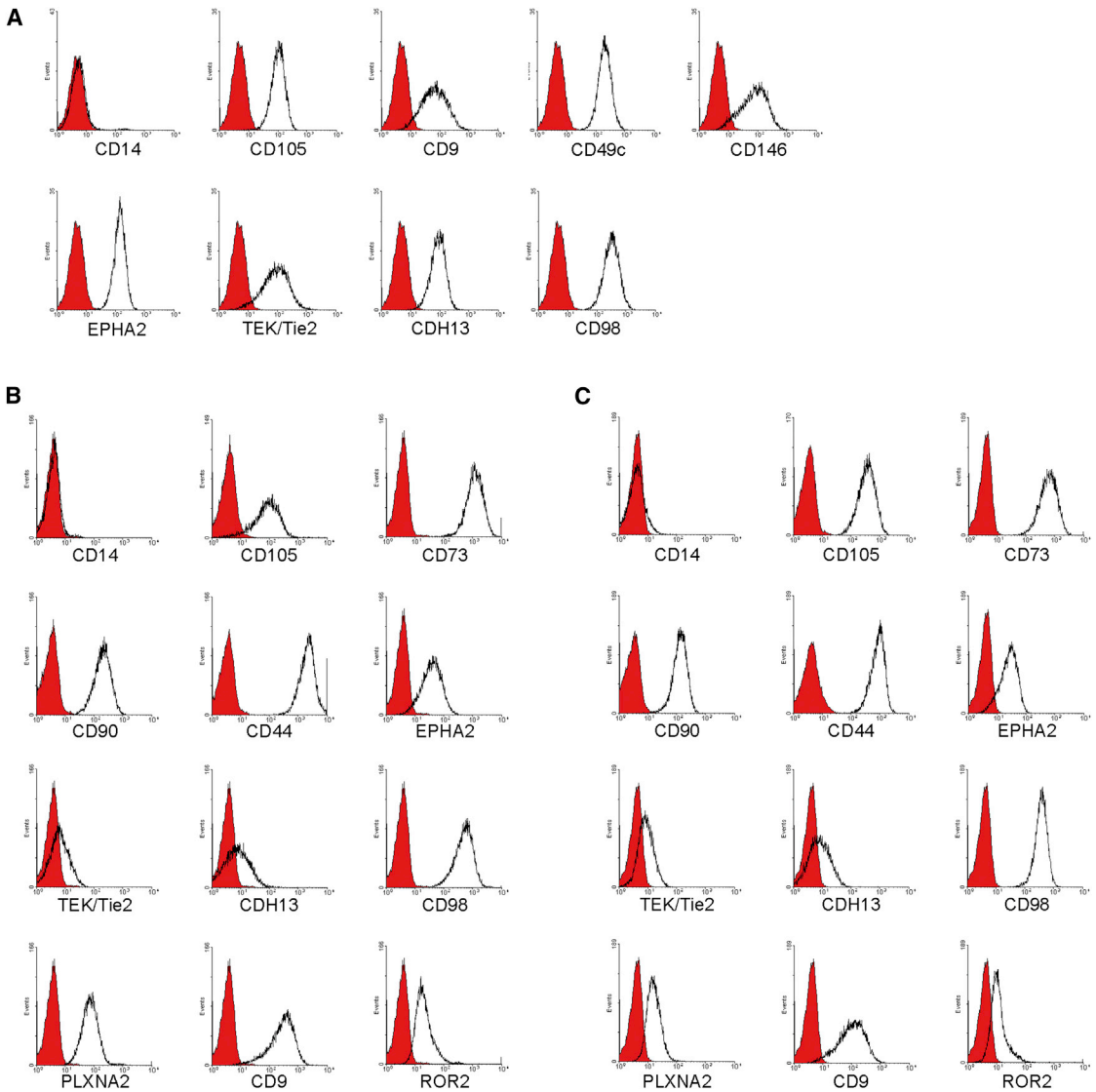

Figure 4. Expression of Markers by Freshly Isolated HUCPVCs, Bone Marrow MSCs, and MSCs from Adipose Tissue

(A) Flow cytometry for the indicated markers using freshly isolated HUCPVCs, at passage 0, after cell release from perivascular regions of the umbilical cord with collagenase. Plots are representative profiles (n = 2 donors). Red filled, isotype control; black line, antibody as indicated.

(B) Flow cytometry for the indicated markers using freshly isolated bone marrow MSCs, at passage 0, after plating of bone marrow cells on tissue culture plastic, analyzing adherent populations. Plots are representative profiles (n = 2 technical repeats). Red filled, isotype control; black line, antibody as indicated. Plots from two further MSC donors at passage 0 are given in Figure S4.

(C) Flow cytometry for the indicated markers using freshly isolated adipose-derived MSCs, at passage 0, after plating of isolated cells from subcutaneous fat on tissue culture plastic, analyzing adherent populations. Plots are representative profiles (n = 2 technical repeats). Red filled, isotype control; black line, antibody as indicated. Plots from two further adipose-derived MSC donors at passage 0 are given in Figure S4.

See also Figure S4.

Effects of Depleting Cell-Interface Markers on Cell Lineage

MSCs can be induced to differentiate in vitro along mesenchymal lineages such as bone, cartilage, tendon, muscle, and fat, and they may also differentiate into non-mesenchymal cells such as neural, endothelial, and SMCs (Ball et al., 2014). qPCR was used to investigate whether knockdown of the selected progenitor cell markers changed gene expression profiles of markers that would indicate differentiation, after siRNA treatment for 12 days (Figures 6H–6O).

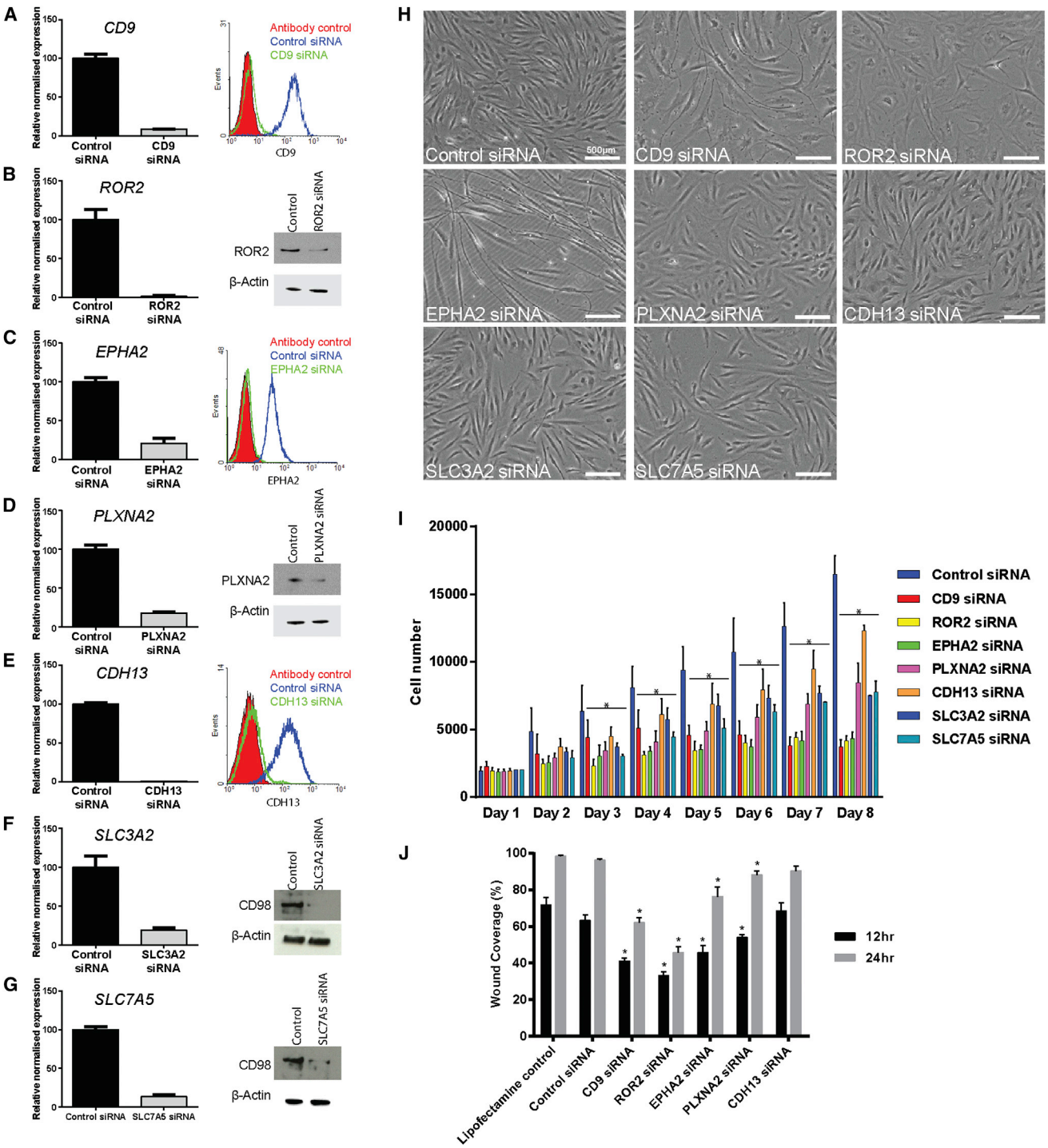

Figure 5. siRNA against Newly Identified Mesenchymal Progenitor Markers Reveals Functional Roles

(A–G) Validation of knockdown using siRNA. (Left) qRT-PCR results for the indicated gene after 24 hr treatment with each siRNA. (Right) Flow cytometry or immunoblots for the protein indicated after 7 days of siRNA treatment (n = 3 independent experiments using two different donor-derived MSC cultures; error bars represent + SD.). Cells were transfected at days 0, 2, and 5.

(H) Phase-contrast images of cells at day 7 after siRNA additions (representative images from three independent experiments all with two different donor-derived MSC cultures). Cells were transfected at days 0, 2, and 5.

(legend continued on next page)

CD9 knockdown resulted in a significant increase in adipogenic markers *C/EBPα*, *FABP4*, and *PPARγ* (Figure 6H). Significant increases in *FABP4* and *PPARγ* were also detectable after EPHA2 siRNA treatment (Figure 6H). In contrast, osteogenic marker expression (*ALPL/Col1a1/RUNX2*) was significantly reduced with EPHA2 and CD9 siRNAs (Figure 6I). EPHA2 knockdown also resulted in significantly reduced expression of the chondrogenic marker *AGGRECAN*, whereas a 68-fold increase in *AGGRECAN* expression was detected after knockdown of CD9 (Figure 6J). Ectodermal markers, *NEUROD2* and *SOX1*, and endodermal marker, *FOXA2*, were also increased in CD9-siRNA-treated cells. Mesodermal markers *ACTA2* and *SNAI1* were significantly downregulated (Figures 6K–6M) in CD9 and EPHA2 knockdown cells (Figure 6M). The osteogenic markers, *COL1A1* and osteocalcin (*BGLAP*), were significantly downregulated in ROR2 and PLXNA2 knockdown cells (Figure 6I), with significant upregulation of ectodermal and endodermal genes in ROR2 siRNA-treated cells (Figures 6K and 6L).

We also investigated whether individual knockdown of mesenchymal markers ROR2, EPHA2, CDH13, or PLXNA2, together with known MSC marker CD9, altered the expression of the other selected multipotency MSC markers (Figures 6N and 6O). At 6 hr after siRNA addition, little effect on expression of the other markers was detectable in each set of knockdown cells, highlighting the specificity of each siRNA (Figure 6N). However, after 3 days or longer, marked alterations in the expression of each of the other genes were detected (Figures 6O and S5B). For example, *CD9* expression was significantly decreased after EPHA2 knockdown, and *EPHA2* mRNA levels were also decreased in CD9 knockdowns (Figures 6O, S5B, and S5C). In addition, *ROR2*, *PLXNA2*, and *CDH13* were reduced after EPHA2 knockdown (Figure 6O). Thus, knockdown of one marker affects the mRNA expression levels of other markers, emphasizing their interlinked roles in mesenchymal progenitor cell biology.

DISCUSSION

Defining the composition of the pericellular interface of mesenchymal progenitor cells is essential to understand their biology and for reproducible therapies. In this study, we defined the cell-surface-matrix proteome of MSCs and HUCPVCs using relative quantitative MS of highly enriched membrane and matrix fractions. Our data reveal many novel surface markers and have shown how these markers affect cell shape, proliferation, and migration. The complexity of the pericellular proteome of mesenchymal progenitor cells revealed by our study provides a basis for future analyses of its functional and therapeutic importance.

To achieve deep proteomic mining, our strategy needed several elements. First, high-quality plasma membrane and matrix-enriched preparations were prepared that enabled the mass spectrometer to detect low level expressed peptides, by reducing background high-abundance peptide interference. This step is essential, as cell-surface biomarkers are often expressed at low copy number. Second, 2D liquid chromatography prior to liquid chromatography-tandem mass spectrometry (LC-MS/MS) enabled tryptic peptides to be sufficiently separated and individually loaded on to the MS instrument. This allowed us to record data on 48,169 peptides for membrane-enriched and 9,970 in matrix-enriched fractions and permitted data integration for high-confidence assignment of peptides to over 6,000 and 1,300 proteins, respectively. Without this level of quantification, test data are relatively intractable. Third, we used eight-channel isobaric tagging to identify lead biomarker candidates with high confidence in relative quantification across samples, which, given the run times needed, would not be possible with label-free methods. Our post-MS validation procedures confirmed the robustness of our approach in identifying new surface proteins of progenitor cells. Importantly, the method allows several samples to be analyzed concurrently to identify variance (e.g., between three HUCPVC populations), which provides exclusion criteria for candidate biomarker selection and avoids identifying donor-specific markers.

Our identification of proteins, with at least a 10-fold improvement in quantification compared with previous published studies, is a major leap in defining the mesenchymal progenitor cell-matrix interface proteome. Other groups have identified similar overall protein numbers and some similar markers when studying MSC populations (Mindaye et al., 2013a, 2013b), but previous attempts at quantifying differences in marker protein levels between cell types have been limited. One study, which used

(I) Cell proliferation assay results. Cells were plated at 1,800 cells per cm^2 and incubated with specific siRNAs for the indicated time periods before assessing cell numbers. Cells were transfected with siRNAs at days 0, 2, 5, and 7. Plots show error bars + SD (n = 4 independent experiments using two different donor-derived MSC cultures). *p < 0.05 compared with control siRNA.
(J) Cell wound assay migration results. Cells were grown to confluency for 5 days with siRNA addition (transfected day 0, 2, and 5) before a single wound was made and wound closure was monitored for 24 hr. Data are represented as percentage wound coverage at 12 and 24 hr after injury. Plots show error bars +SD (n = 4 independent experiments using two different donor-derived MSC cultures). *p < 0.05 compared with control siRNA.

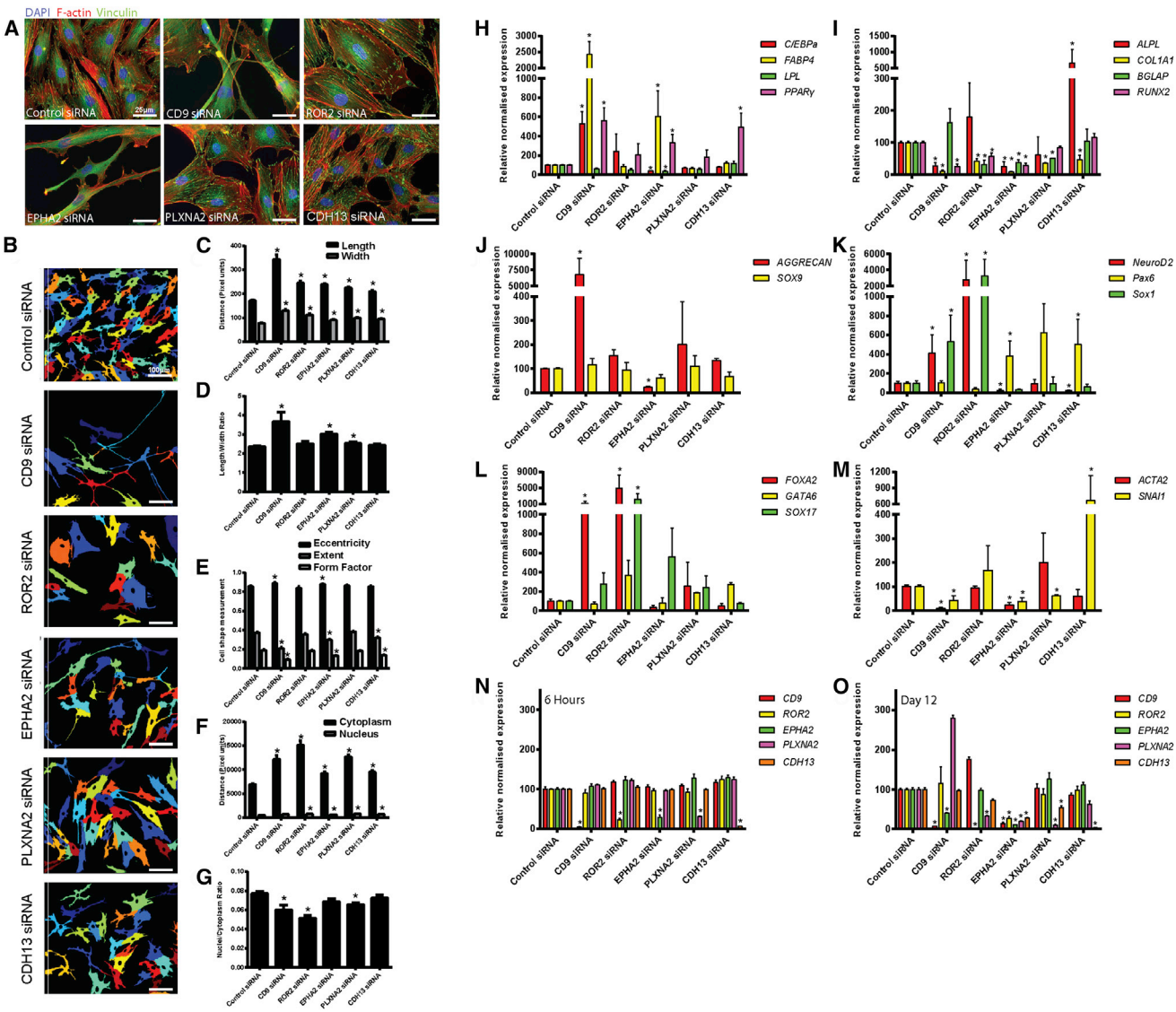

Figure 6. Mesenchymal Progenitor Cell Marker siRNAs Affect Focal Adhesion Formation, Cell Shape, and Gene Expression Profiles of MSCs

(A) Representative immunofluorescence staining for vinculin (green), F-actin (red), and nuclei (DAPI, blue) after siRNA treatment for 7 days (n = 3 independent experiments using two different donor-derived MSC cultures). Cells were plated at equivalent densities 48 hr prior to imaging.

(B–G) Cell image processing to determine the size and shape measurements of MSCs after staining with wheat germ agglutinin, F-actin, and DAPI on day 7 of siRNA-treated cultures plated at equivalent densities 24 hr prior to imaging (B). Processed CellProfiler output files determining cell boundaries are shown. Full images are shown in Figure S5A. Representative length and width measurements (C), length to width ratios (D), cytoplasm and nuclei measurements (E), nucleus to cytoplasm ratios (F) and two distinct shape features, eccentricity, extent, and form factor (G) taken from six to ten processed images from two independent experiments both using two different MSC cultures (n = 4). Plots show error bars + SEM. *p < 0.05 compared with control siRNA.

(H–M) qRT-PCR to define the changes in expression of adiopogenic (H), osteogenic (I), chondrogenic (J), ectodermal (K), endodermal (L), and mesodermal (M) markers after siRNA treatment for 12 days under multipotent growth conditions relative to control siRNA treated cultures (n = 4 from two independent experiments using two different donor-derived MSCs). Plots show error bars + SD.

(N and O) Expression of *CD9*, *ROR2*, *EPHA2*, *PLXNA2*, and *CDH13* after treatment with the indicated siRNA for 6 hr (N) or 12 days (O) relative to control siRNA. Expression is normalized to housekeeper genes *TBP* and *β2M*. Error bars + SEM (n = 4 from two independent experiments using two different donor-derived MSCs); *p < 0.05 compared with control siRNA.

See also Figure S5.

isotypic cysteine labeling to compare bone marrow and umbilical cord vein mesenchymal progenitor cells, enabled the quantification of 545 proteins, but represented a global proteomic approach with no pre-fractionation of membrane proteins prior to LC-MS/MS (Miranda et al., 2012). Using iTRAQ to simultaneously deliver relative quantification of multiple samples has major advantages over other MS methods for analyzing the membrane proteome, which are often poorly resolved using gel-based methods and, in the case of 2D-PAGE MS comparisons, rely on visible differences in silver stain intensity prior to protein identification (Kim et al., 2012).

The identification of known MSC markers within our panel of biomarkers endorses our method, with validation by flow cytometry or immunoblotting, confirming that the markers are largely restricted to MSCs and HUCPVCs. Further confirmation of their selective expression by mesenchymal progenitor cells was demonstrated using fresh bone marrow aspirates and adipose-derived MSC cultures. Knockdown experiments on selected markers demonstrated that each influences MSC fate, exerting differential effects on cell shape, proliferation, and migration and on expression of both known progenitor/differentiated cell markers and the progenitor-specific molecules identified here.

Progenitor cells from different tissue sources can exhibit phenotypic variations. Here, we have identified a number of cell-type-specific differences between MSCs and HUCPVCs; however, the fact that only 11 proteins were upregulated in one progenitor cell type and downregulated in the other strongly suggests that these cells are functionally related. Nevertheless, it will be interesting to investigate further the HUCPVC- and MSC-specific proteins in order to define their cellular roles.

We and others have shown that protein and mRNA levels are not directly comparable (Miranda et al., 2012; Unwin and Whetton, 2006). Although published transcriptomic analyses comparing bone marrow MSCs with HDFs have identified some similar markers to those identified in this study, e.g., enrichment in *ADAM12*, *VCAM1*, and *ALPL* (Ren et al., 2011), there were also marked variations, underlining the essential need to define protein levels.

Although well beyond the remit of this study to define the full significance of the expression of all identified MSC markers, we conducted selected knockdowns to gain initial insights. Knockdown of CD9, ROR2, and EPHA2 resulted in dramatic alterations in MSC phenotype. Comparable siRNA analyses of HUCPVC donor cultures showed similar results (unpublished data). CD9 is a tetraspanin receptor that interacts with and activates β1 integrin adhesion receptors, altering integrin-dependent cell migration (Kotha et al., 2008). Although CD9 is widely reported to be expressed by mesenchymal progenitor cells from different tissues and to influence integrin signaling, investigations into its function in MSCs are limited. We found that depletion of CD9 alters MSC proliferation, shape, and migration and blocks focal adhesions, thereby modifying cell fate.

ROR2 is a member of an orphan receptor tyrosine kinase family. *Ror2*-deficient mice are neonatal lethal due to severe skeletal and heart defects (Takeuchi et al., 2000). Mutations in *Ror2* in humans cause skeletal dysplasias (Afzal and Jeffery, 2003). ROR2 has been proposed to regulate osteogenic differentiation of MSCs in vitro possibly by acting as a Wnt co-receptor (Yun et al., 2014). We have shown that depletion of ROR2 not only downregulates osteogenic markers (COL1A1, BGLAP, RUNX2) in multipotent growth conditions, but also dramatically changes cell shape and inhibits cell proliferation and migration, suggesting that ROR2 crosstalk with Wnts may regulate mesodermal development.

EPHA2 is a member of the family of Eph receptor tyrosine kinases that influence development and is often deregulated in cancer cells. It binds membrane-bound ephrin-A family ligands residing on adjacent cells, leading to contact-dependent bidirectional signaling that can modulate expression of mesodermal genes. EPHA2 may negatively regulate cell-ECM adhesion and cell growth due to suppression of focal adhesion kinase (Miao et al., 2000), whereas others have shown that ephrin-A-EphA2 signaling promotes FAK- and p130cas-dependent cell adhesion and cytoskeletal assembly (Carter et al., 2002). In agreement with the latter study, downregulation of EPHA2 in MSCs reduced focal adhesion formation, altering cell shape, inhibiting migration, and downregulating mesodermal gene expression. Similarities in knockdown phenotypes of CD9 and EPHA2 suggest that these proteins may function in overlapping pathways to maintain MSC fate.

In summary, we have applied state-of-the-art quantitative proteomics to define the cell-matrix interface of multipotent mesenchymal progenitor cells and identify markers that influence cell fate. As well as the universal applicability of this approach to stem cell analysis, our proteomic data deliver a step advance toward improved therapeutic MSC applications by providing a basis for better selection and understanding of their biology.

EXPERIMENTAL PROCEDURES

Cells and Cell Culture

MSCs (donors: 7F3674 [22-year-old black female], 6F4085 [33-year-old black male], 183402 [21-year-old white female], and 6F3502 [21-year-old black male], all purchased from Lonza at passage 2) were cultured on gelatin-coated plastic in MesenPRO RS Medium (Gibco), essentially as described (Ball et al., 2012). In brief, cells cryo preserved at P2 were expanded at a ratio of 1:5 when ~90%

confluent and used in all experiments at passage 5. This protocol was needed to provide sufficient cells for the proteomic analysis and validation experiments. HUCPVCs from six donors isolated as described (Sarugaser et al., 2005) (gift from Professor J. E. Davies, University of Toronto) were cultured in alpha-minimum essential medium (α-MEM) (Sigma), 10% v/v batch-tested fetal calf serum (FCS), and 2 mM L-glutamine and used at passage 0 (outgrowth from primary tissue) or passage 6. Matched adipose-derived MSCs and bone marrow-MSCs from four donors were isolated from subcutaneous fat and bone marrow removed from the proximal femur during hip-replacement surgery (average age 54 years [47 to 61 years]; two women and two men) as previously described (Strassburg et al., 2010). Cells were obtained in accordance with local ethical approval and with the fully informed consent of patients. Cells were either used for flow cytometry immediately (freshly isolated mononuclear cells) or plated in α-MEM with 20% FCS, discarding non-adherent cells after 5 days and retaining adherent cells for flow cytometric analysis at passage 0. Adult HDFs (Cascade Biologic) from three donors were cultured in Dulbecco's modified Eagle's medium (Biowhittaker), 10% FCS, L-glutamine and used at passage 6. Differentiation toward adipogenic, osteogenic, or chondrogenic lineages was performed using defined differentiation media and cell identification methods (RnD Systems/StemPro). HUVECs were maintained in Endothelial Cell Growth Medium (Promocell). Passage 5 aortic SMCs and coronary artery SMCs were maintained in Medium 231 supplemented with smooth muscle growth supplement (Life Technologies) and L-glutamine.

Flow Cytometry

Cells were collected after detachment with cell dissociation buffer or trypsin and processed for flow cytometry. For details of antibodies, see Supplemental Experimental Procedures. Samples were analyzed using a Beckman Coulter Cyan ADP and Summit v.4.3 software, or BD FACSCanto using BD FACSDIVA software processing with WinMidi 2.8.

Preparation of Enriched Plasma Membranes

Cells were grown to 90% confluence, washed in PBS, and collected by gentle scraping. Cells were pelleted at 800 *g* for 3 min, washed in PBS, repelleted, and resuspended in precooled lysis buffer (10 mM HEPES/1 mM EDTA/pH 7.5/1X protease inhibitors; Sigma) at 10^7 cells/ml and disrupted with a dounce homogenizer. Cells were centrifuged (10 min, 500 *g*) to pellet the nucleus. Membranes were enriched as described (Holland et al., 2011), with slight modification as described in the Supplemental Experimental Procedures.

Preparation of Pericellular Matrix-Enriched Preparations

Cells grown to confluence were washed with PBS (no Ca/Mg). Lysis buffer (20 mM NH_4OH/0.5% NP40/PBS) was added to the cell layer and incubated at room temperature until cells detached (~5 min). Remaining matrix was washed in PBS+Ca/Mg and then incubated with benzonase (25 U/ml; Merck)/PBS + Ca^{2+}/Mg^{2+} at 37°C for 30 min, before washing with PBS. Matrix was solubilized in 0.5 M triethyl ammonium bicarbonate (TEAB)/0.05% SDS/protease inhibitors and incubated at 70°C for 30 min. Insoluble material was removed by centrifugation.

iTRAQ Labeling and MS

Protein (100 μg) from each sample underwent reduction in 0.1 volumes of 50 mM tris-(2-carboxyethyl) phosphine (Sigma) at 60°C for 1 hr. Reduced cysteine residues were alkylated using 0.05 volumes of 200 mM methylmethanethiosulphate/isopropanol (Thermo Fisher Scientific). Protein samples were digested with trypsin (1:10, enzyme:protein) at 37°C overnight before labeling with iTRAQ reagent (Applied Biosystems). Samples were pooled prior to MS analysis, as detailed in the Supplemental Experimental Procedures.

Immunoblotting

For whole-cell lysates, cells were washed with PBS and scraped into RIPA buffer (Sigma)/protease inhibitors and centrifuged at 14,000 *g*, 10 min, 4°C. Protein concentration was determined using the Pierce BCA protein assay. For immunoblotting, 2- to 20-μg protein was loaded per well of an SDS-PAGE gel and then immunoblotted as described (Ball et al., 2004). For antibodies, see the Supplemental Experimental Procedures. Instant*Blue* (Expedeon) was used for Coomassie blue staining. GeneTools (Syngene) was used for quantification.

RNA Isolation and qRT-PCR

RNA was isolated using the ReliaPrep RNA Miniprep System (Promega) and converted into cDNA using the Tetro cDNA Synthesis Kit (Bioline). qPCR was performed using the GoTaq qPCR kit (Promega) on a Bio-Rad CFX touch 1000 qPCR machine. Gene expression was normalized relative to housekeeping genes *TBP* and *β2M*. Expression relative to control was determined using the ΔCt method using Bio-Rad CFX Manager software. Primers are listed in the Supplemental Experimental Procedures; QuantiTect Primer Assays (QIAGEN) were used for unlisted genes.

siRNA Experiments

GeneSolution siRNAs were purchased from QIAGEN. siRNAs were used at a final concentration of 40 nM. Lipofectamine RNAiMAX transfection reagent (Invitrogen) was used, transfecting cells every 2 to 3 days.

Cell Proliferation Assay

Cells were plated at 1,800 cells per cm^2, and siRNA transfections were performed as described. Cell density was measured every 24 hr using the CyQUANT Cell Proliferation Assay (Life Technologies).

Migration Assay

MSCs were plated at 6,000 cells/cm^2 and transfected with siRNAs as described. On day 5, a wound was made using a pipette tip, and plates were imaged using an inverted live cell imaging microscope (20×/0.5 HC Plan Fluotar objective, Leica DMIRE), maintained at 37°C/5% CO_2 in a humidified atmosphere. A motorized XYZ stage allowed multiple positions to be imaged, collecting images every 10 min over 24 hr through Image Pro 6.3 software (Media Cybernetics).

Immunofluorescence Staining

Cells were fixed with 4% paraformaldehyde and processed for immunofluorescence staining. Antibodies/dyes are listed in the Supplemental Experimental Procedures. Images were captured on an Olympus BX51 upright microscope using a Coolsnap ES camera (Photometrics) through MetaVue Software (Molecular Devices). Images were processed and analyzed using ImageJ (http://rsb.info.nih.gov/ij). Cell shape measurements used CellProfiler image analysis software (Carpenter et al., 2006) as described (Ball et al., 2012).

Statistical Analyses

A Student's t test or two-way ANOVA was used to calculate significance using a p value of less than 0.05.

SUPPLEMENTAL INFORMATION

Supplemental Information includes Supplemental Experimental Procedures, five figures, and seven tables and can be found with this article online at http://dx.doi.org/10.1016/j.stemcr.2015.01.007.

ACKNOWLEDGMENTS

This work was co-funded by the Medical Research Council and British Heart Foundation G0902170 (R.J.H., G.T., C.L.R.M., A.D.W., C.M.K., and A.E.C.). S.A.C. is funded by UK Regenerative Medicine Platform. A.J.K.W. and A.D.W. were supported by Leukaemia Lymphoma Research. The Bioimaging Facility microscopes were funded by the BBSRC, Wellcome Trust, and University of Manchester. We thank Dr. S.G. Ball for experimental advice and Professor J.E. Davies (University of Toronto) for provision of HUCPVCs.

Received: May 23, 2014
Revised: January 12, 2015
Accepted: January 12, 2015
Published: February 12, 2015

REFERENCES

Afzal, A.R., and Jeffery, S. (2003). One gene, two phenotypes: ROR2 mutations in autosomal recessive Robinow syndrome and autosomal dominant brachydactyly type B. Hum. Mutat. *22*, 1–11.

Ball, S.G., Shuttleworth, A.C., and Kielty, C.M. (2004). Direct cell contact influences bone marrow mesenchymal stem cell fate. Int. J. Biochem. Cell Biol. *36*, 714–727.

Ball, S.G., Shuttleworth, A., and Kielty, C.M. (2012). Inhibition of platelet-derived growth factor receptor signaling regulates Oct4 and Nanog expression, cell shape, and mesenchymal stem cell potency. Stem Cells *30*, 548–560.

Ball, S.G., Worthington, J.J., Canfield, A.E., Merry, C.L., and Kielty, C.M. (2014). Mesenchymal stromal cells: inhibiting PDGF receptors or depleting fibronectin induces mesodermal progenitors with endothelial potential. Stem Cells *32*, 694–705.

Batsali, A.K., Kastrinaki, M.C., Papadaki, H.A., and Pontikoglou, C. (2013). Mesenchymal stem cells derived from Wharton's Jelly of the umbilical cord: biological properties and emerging clinical applications. Curr. Stem Cell Res. Ther. *8*, 144–155.

Cai, J., Miao, X., Li, Y., Smith, C., Tsang, K., Cheng, L., and Wang, Q.F. (2014). Whole-genome sequencing identifies genetic variances in culture-expanded human mesenchymal stem cells. Stem Cell Rep. *3*, 227–233.

Carpenter, A.E., Jones, T.R., Lamprecht, M.R., Clarke, C., Kang, I.H., Friman, O., Guertin, D.A., Chang, J.H., Lindquist, R.A., Moffat, J., et al. (2006). CellProfiler: image analysis software for identifying and quantifying cell phenotypes. Genome Biol. *7*, R100.

Carter, N., Nakamoto, T., Hirai, H., and Hunter, T. (2002). EphrinA1-induced cytoskeletal re-organization requires FAK and p130(cas). Nat. Cell Biol. *4*, 565–573.

Delorme, B., Ringe, J., Gallay, N., Le Vern, Y., Kerboeuf, D., Jorgensen, C., Rosset, P., Sensebé, L., Layrolle, P., Häupl, T., and Charbord, P. (2008). Specific plasma membrane protein phenotype of culture-amplified and native human bone marrow mesenchymal stem cells. Blood *111*, 2631–2635.

Ennis, J., Sarugaser, R., Gomez, A., Baksh, D., and Davies, J.E. (2008). Isolation, characterization, and differentiation of human umbilical cord perivascular cells (HUCPVCs). Methods Cell Biol. *86*, 121–136.

Foster, L.J., Zeemann, P.A., Li, C., Mann, M., Jensen, O.N., and Kassem, M. (2005). Differential expression profiling of membrane proteins by quantitative proteomics in a human mesenchymal stem cell line undergoing osteoblast differentiation. Stem Cells *23*, 1367–1377.

Holland, M., Castro, F.V., Alexander, S., Smith, D., Liu, J., Walker, M., Bitton, D., Mulryan, K., Ashton, G., Blaylock, M., et al. (2011). RAC2, AEP, and ICAM1 expression are associated with CNS disease in a mouse model of pre-B childhood acute lymphoblastic leukemia. Blood *118*, 638–649.

Honmou, O., Onodera, R., Sasaki, M., Waxman, S.G., and Kocsis, J.D. (2012). Mesenchymal stem cells: therapeutic outlook for stroke. Trends Mol. Med. *18*, 292–297.

Kim, J., Shin, J.M., Jeon, Y.J., Chung, H.M., and Chae, J.I. (2012). Proteomic validation of multifunctional molecules in mesenchymal stem cells derived from human bone marrow, umbilical cord blood and peripheral blood. PLoS ONE *7*, e32350.

Kim, N., Im, K.I., Lim, J.Y., Jeon, E.J., Nam, Y.S., Kim, E.J., and Cho, S.G. (2013). Mesenchymal stem cells for the treatment and prevention of graft-versus-host disease: experiments and practice. Ann. Hematol. *92*, 1295–1308.

Kotha, J., Longhurst, C., Appling, W., and Jennings, L.K. (2008). Tetraspanin CD9 regulates beta 1 integrin activation and enhances cell motility to fibronectin via a PI-3 kinase-dependent pathway. Exp. Cell Res. *314*, 1811–1822.

Lee, R.H., Pulin, A.A., Seo, M.J., Kota, D.J., Ylostalo, J., Larson, B.L., Semprun-Prieto, L., Delafontaine, P., and Prockop, D.J. (2009). Intravenous hMSCs improve myocardial infarction in mice because cells embolized in lung are activated to secrete the anti-inflammatory protein TSG-6. Cell Stem Cell *5*, 54–63.

Mareddy, S., Broadbent, J., Crawford, R., and Xiao, Y. (2009). Proteomic profiling of distinct clonal populations of bone marrow mesenchymal stem cells. J. Cell. Biochem. *106*, 776–786.

Miao, H., Burnett, E., Kinch, M., Simon, E., and Wang, B. (2000). Activation of EphA2 kinase suppresses integrin function and

causes focal-adhesion-kinase dephosphorylation. Nat. Cell Biol. *2*, 62–69.

Mindaye, S.T., Ra, M., Lo Surdo, J., Bauer, S.R., and Alterman, M.A. (2013a). Improved proteomic profiling of the cell surface of culture-expanded human bone marrow multipotent stromal cells. J. Proteomics *78*, 1–14.

Mindaye, S.T., Ra, M., Lo Surdo, J.L., Bauer, S.R., and Alterman, M.A. (2013b). Global proteomic signature of undifferentiated human bone marrow stromal cells: evidence for donor-to-donor proteome heterogeneity. Stem Cell Res. (Amst.) *11*, 793–805.

Miranda, H.C., Herai, R.H., Thomé, C.H., Gomes, G.G., Panepucci, R.A., Orellana, M.D., Covas, D.T., Muotri, A.R., Greene, L.J., and Faça, V.M. (2012). A quantitative proteomic and transcriptomic comparison of human mesenchymal stem cells from bone marrow and umbilical cord vein. Proteomics *12*, 2607–2617.

Panepucci, R.A., Siufi, J.L., Silva, W.A., Jr., Proto-Siquiera, R., Neder, L., Orellana, M., Rocha, V., Covas, D.T., and Zago, M.A. (2004). Comparison of gene expression of umbilical cord vein and bone marrow-derived mesenchymal stem cells. Stem Cells *22*, 1263–1278.

Pittenger, M.F., Mackay, A.M., Beck, S.C., Jaiswal, R.K., Douglas, R., Mosca, J.D., Moorman, M.A., Simonetti, D.W., Craig, S., and Marshak, D.R. (1999). Multilineage potential of adult human mesenchymal stem cells. Science *284*, 143–147.

Prockop, D.J. (2013). Concise review: two negative feedback loops place mesenchymal stem/stromal cells at the center of early regulators of inflammation. Stem Cells *31*, 2042–2046.

Ren, J., Jin, P., Sabatino, M., Balakumaran, A., Feng, J., Kuznetsov, S.A., Klein, H.G., Robey, P.G., and Stroncek, D.F. (2011). Global transcriptome analysis of human bone marrow stromal cells (BMSC) reveals proliferative, mobile and interactive cells that produce abundant extracellular matrix proteins, some of which may affect BMSC potency. Cytotherapy *13*, 661–674.

Sarugaser, R., Lickorish, D., Baksh, D., Hosseini, M.M., and Davies, J.E. (2005). Human umbilical cord perivascular (HUCPV) cells: a source of mesenchymal progenitors. Stem Cells *23*, 220–229.

Soteriou, D., Iskender, B., Byron, A., Humphries, J.D., Borg-Bartolo, S., Haddock, M.C., Baxter, M.A., Knight, D., Humphries, M.J., and Kimber, S.J. (2013). Comparative proteomic analysis of supportive and unsupportive extracellular matrix substrates for human embryonic stem cell maintenance. J. Biol. Chem. *288*, 18716–18731.

Strassburg, S., Richardson, S.M., Freemont, A.J., and Hoyland, J.A. (2010). Co-culture induces mesenchymal stem cell differentiation and modulation of the degenerate human nucleus pulposus cell phenotype. Regen. Med. *5*, 701–711.

Takeuchi, S., Takeda, K., Oishi, I., Nomi, M., Ikeya, M., Itoh, K., Tamura, S., Ueda, T., Hatta, T., Otani, H., et al. (2000). Mouse Ror2 receptor tyrosine kinase is required for the heart development and limb formation. Genes Cells *5*, 71–78.

Unwin, R.D., and Whetton, A.D. (2006). Systematic proteome and transcriptome analysis of stem cell populations. Cell Cycle *5*, 1587–1591.

Weekes, M.P., Antrobus, R., Lill, J.R., Duncan, L.M., Hör, S., and Lehner, P.J. (2010). Comparative analysis of techniques to purify plasma membrane proteins. J. Biomol. Tech. *21*, 108–115.

Yun, K., Ajima, R., Sharma, N., Costantini, F., Mackem, S., Lewandoski, M., Yamaguchi, T.P., and Perantoni, A.O. (2014). Noncanonical Wnt5a/Ror2 signaling regulates kidney morphogenesis by controlling intermediate mesoderm extension. Hum. Mol. Genet. *23*, 6807–6814.